W与 Cu合金瞬时液相连接分析

沈以赴[1], 刘仕福[1], 李军伟[2], 徐 杰[1]
(1.南京航空航天大学 材料科学与技术学院, 南京 210016; 2.厦门虹鹭公司 厦门 361021)

摘 要: 采用金属粉末 67Cu-33Mn, 67Cu-33Mn-5Ni(质量百分比)为中间层对 W与 Cu合金进行了瞬时液相连接, 利用 SEM、EDX分别对试样进行显微组织及成分分析, 并探讨其连接机理。结果表明, 中间层 67Cu-33Mn-5Ni获得的接头比中间层 67Cu-33Mn的显微组织更致密, 结合性更好。分析认为, Ni的加入, 提高了中间层溶质的扩散率, 加速了液相的等温凝固; Ni还溶解一定量的 W, 形成 Ni(W)固溶体。其连接机理是通过中间层 Cu-Mn形成液相, 与母材 Cu实现瞬时液相连接; 与母材 W实现钎焊连接。

关键词: 瞬时液相连接; 钎焊; 显微组织; 机理
中图分类号: TG457 文献标识码: A 文章编号: 0253-360X(2005)12-73-04

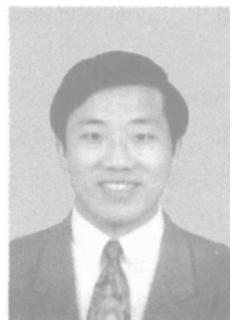

沈以赴

0 序 言

钨(W)因熔点高(3 410 ℃)、抗腐蚀性能好等优点, 而常选作为耐高温材料; Cu及其合金因高热导率(400W/mK)特点, 而往往选作为散热材料。如今, 在很多工程应用中, 更需要材料既具有耐高温性能又具有良好的热传导性能, 如热核聚变装置中的面向等离子体元件[1]。然而, 现有材料很难完全同时满足上述两种性能。因此, 需要可靠的连接技术将 W与 Cu及其合金连接起来。

W与 Cu合金连接的最大问题是 W与 Cu合金间热膨胀系数差别大($\alpha_{Cu}=4\alpha_w$), 在高温连接时会产生很大的残余应力, 严重时将使接头开裂[2]。另外, W与 Cu既不互溶, 也不形成金属间化合物, 很难直接连接。为了解决 W与 Cu合金连接难点, 国内外对 W与 Cu合金连接进行了大量的研究。目前, W与 Cu合金连接技术主要有扩散焊, 活性钎焊及活性金属浇注法(active metal casting)。在扩散焊过程中, 往往需要在 W与 Cu合金间夹中间层, 如 OFHC-Cu[3~6]、Ti/Ni[7]、OFHC-Cu/Au[3]、、Ni/OFHC-Cu、Ti/OFHC-Cu[5,7]、Ti/Ni/Ti[8]; 钎焊常用钎料有 Cu-Mn合金[9]及 Ag-Cu合金[10]; 活性浇注法[4]是 Plansee公司专门为 W与 Cu合金连接而发明的一种连接方法。尽管 W与 Cu合金连接技术研究很多, 由于该技术涉及到保密性, 向外报道甚少。因此, 开展 W与 Cu及其合金连接技术研究是十分必要的。

文中采用瞬时液相(transient liquid phase, TLP)连接技术对 W与 Cu合金进行连接试验研究。通过自配 Cu、Mn金属粉末作中间层, 并合理地制定连接工艺, 成功地实现了 W与 Cu合金的 TLP连接。

1 试验材料及方法

1.1 试验材料

焊接母材为 W和黄铜(H62), 尺寸为 Φ14 mm×7 mm, 在进行连接试验前, 对母材的受焊表面用 SiC砂纸打磨, 并抛光, 以除去表面氧化物及突出物。然后, 用丙酮及酒精对受焊表面进行反复擦洗, 以除去表面油污。采用金属粉末成分为 67Cu-33Mn、67Cu-33Mn-5Ni(质量分数, %)作为中间层, 其中 Cu、Ni纯度均为 99.99%、颗粒直径为 47 μm; Mn纯度为 99.6%、颗粒直径为 75 μm; 将配比好的金属粉末装进普通卧式球磨机中球磨 3 h, 使混粉均匀。

1.2 试验工艺

W与 Cu合金连接试验是在真空热压炉中进行。按"三明治"式放置(图 1)放入真空热压炉中。升温过程中, 按先加压后升温模式操作, 恒压为 3MPa。在 0~450 ℃温度间, 升温速率为 20 ℃/min, 在 450 ℃保温 30 min; 450~890 ℃升温速率为

收稿日期: 2005-10-31

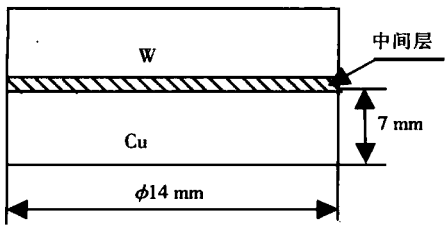

图 1 “三明治”式放置连接试样

Fig. 1 Schematic diagram of bonded specimen

30 ℃ /min, 保温 480 min; 降温过程中, 待炉温降至 450 ℃时, 开始卸压, 其后随炉冷却至室温。工艺曲线及相关参数如图 2所示。在连接温度下真空度优于 5×10^{-3} Pa。

1.3 测 试

利用 QUANT200型扫描电镜对连接界面的微观组织形貌进行观察; 采用 EDAX型能谱仪对界面两侧区域元素进行分析。

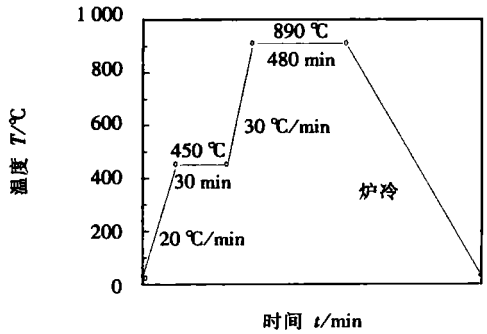

图 2 TLP连接工艺参数

Fig. 2 Schematic of TLP bonding cycle

2 试验结果与讨论

2.1 显微组织分析

图 3为金属粉末 67Cu – 33Mn(质量分数, %)作中间层 TLP接头界面微观组织及成分分布图。从图 3a可知, 中间层是 CuMn固溶体, 在靠母材 Cu侧有跨界面晶粒存在, 靠母材 W侧界面模糊。还发现, 中间层距离母材 Cu越近, 中间层就越致密, 表明了这部分中间层优先熔化、优先等温凝固及均匀化, 因为该部分降熔元素 (melting point depressant) 更容易向母材 Cu扩散。由图 3b可知, 中间层降熔元素 Mn向母材 Cu侧扩散较充分, 向母材 W侧扩散不充分, 这与物质的晶体结构有关。在文献 [11] 中指出, W是体心立方, 原子半径为 0.137 nm, Cu是面心立方, 原子半径为 0.128 nm, Mn是面心立方, 原子半径 0.112 nm。W与 Cu晶体结构不同, 原子半径接近; Cu与 Mn晶体结构相同, 原子半径相差较大。根据相似相容性及置换扩散激活能大于间隙扩散的理论, 论证了试验结果的合理性。

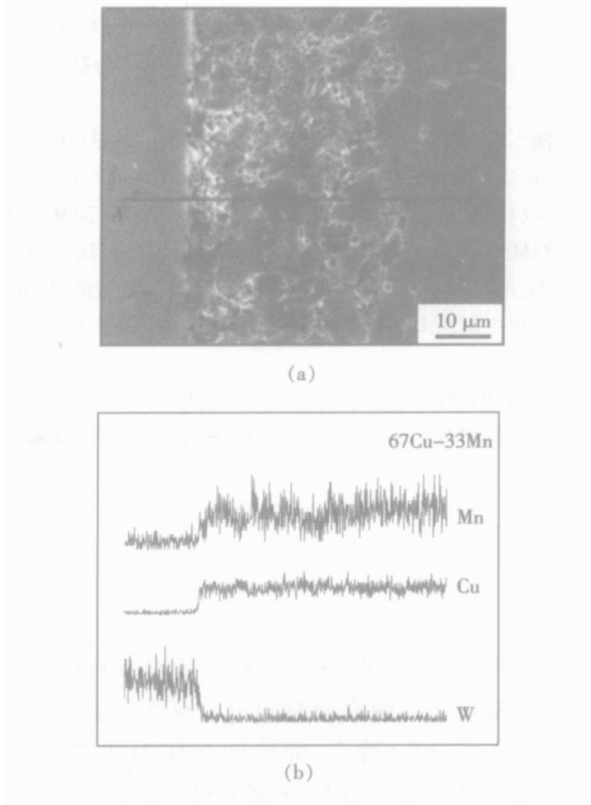

图 3 用 67Cu – 33Mn作中间层 TLP试样接头微观组织和元素分布图

Fig. 3 Microstructure and element distrbution of TLP joint using 67Cu 33Mn as interlayer

图 4为 67Cu – 33Mn – 5Ni(质量分数, %)金属粉末作中间层接头显微微观组织及成分分布图。对比图 3, 中间层仍为 CuMn固溶体, 显微组织更致密, 与母材 Cu的界面几乎消失。在中间层中, 元素 Mn峰值虽然较低, 但仍然看出焊缝中 Mn含量高于 Cu侧; 而元素 Cu峰值也明显提高, 说明母材 Cu中的 Cu元素向焊缝 (CuMn)扩散得到了加强, 即 Ni元素的加入大大增强了母材中的 Cu元素向焊缝的扩散。因此, 组织更致密, 成分更均匀, 接头性能更良好。

图 5为图 4中区域 C的主要化学成分面扫描的结果。由图 5可知, Cu、W元素的峰值非常高, 说明这两种元素量较多, 而 Ni元素明显存在。Ni元素的存在对接头的组织及结合情况均有很大的影响。一方面, Ni会提高 Cu元素向焊缝扩散的扩散率, 使得 Cu、Mn扩散加快, Cu的浓度也随之增加, 其结果是增加了液相量, 加速了等温凝固, 增加接头均匀化

时间，致使获得良好的接头；另一方面，Ni能溶解一定量的 W，形成 Ni(W)固溶体，提高了中间层与母材 W 界面的结合力。有研究表明[12]：随着时间延长，Ni基固溶体溶解 W 将达到饱和，Ni与 W 会进一步形成 NiW$_2$、Ni$_4$W 和 Ni$_6$W 金属间化合物，由于 Ni元素在中间层中的含量较少，形成的金属间化合物也很少，这不仅不会削弱接头力学性能，反而有可能会作为增强相改善接头性能。此外，Ni元素的加入还利于接头的使用温度的提高。

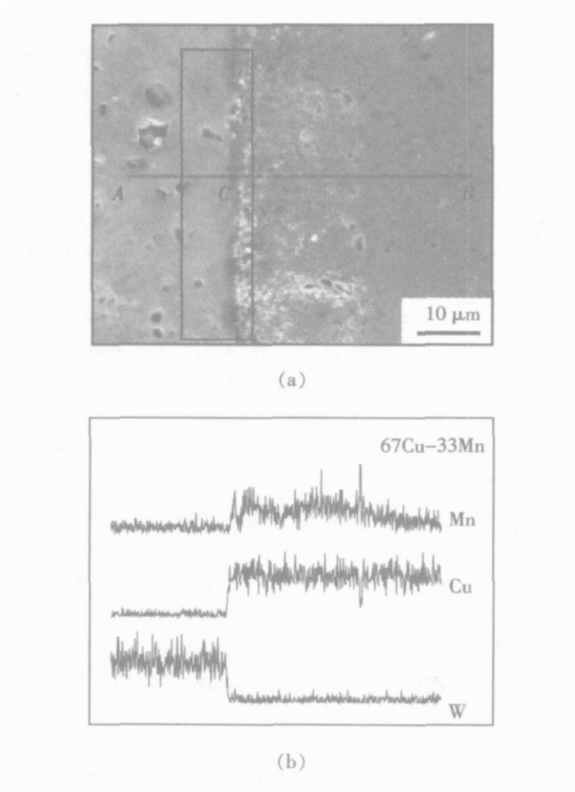

图 4　用 67Cu－33Mn－5Ni作中间层 TLP试样接头微观组织和元素分布图

Fig. 4　Microstructure and element distrbution of TLP joint using 67Cu-33Mn-5Ni as interlayer

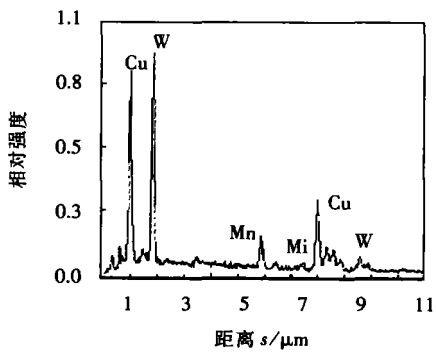

图 5　图 4中 C 区域面扫描图

Fig. 5　Element distrbution of C zone in Fig. 4

2.2　连接机理

根据 Cu－Mn二元合金相图(图 6)可知，Cu、Mn形成液相最低温度 T 为 871 ℃，试验选用温度为 890 ℃，高于 T，且中间层成分恰好约为 T时的质量百分比即 Cu∶Mn＝67∶33。因此，在 W 与 Cu合金 TLP连接过程中，该两种中间层都可以通过晶界及晶粒相互扩散完全形成液相。液相 CuMn在母材 W 与 Cu合金界面间存在，有利于提高中间层与母材 W 侧间结合力；同时也加快了中间层与母材 Cu的互扩散，使中间层与母材 Cu成为整体(见图 3、图 4)，大大提高了与母材 Cu侧的接合强度。另外，瞬时液相的存在还可以使中间层粉末颗粒重排，促使中间层组织更致密，获得良好的接头。

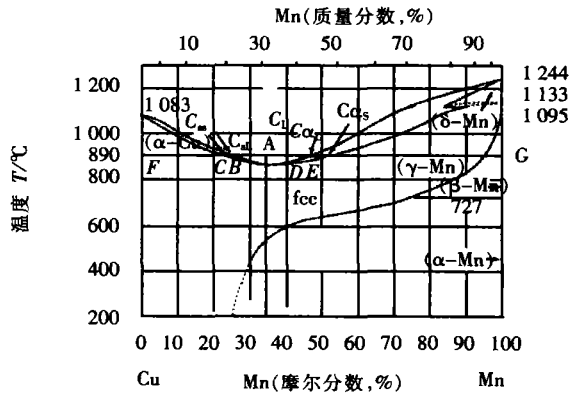

图 6　Cu－Mn二元相图

Fig. 6　Cu-Mn binary phase diagram

瞬时液相(TLP)扩散 W 与 Cu合金连接可划分成两部分来分析，与母材 W 连接主要是机械咬合作用，实质就是钎焊连接；与母材 Cu连接，是通过母材 Cu及中间层 Cu、Mn的相互作用来实现，是典型的 TLP连接机理，其连接过程如下。

(1)中间层熔化阶段：TLP连接开始时，母材 Cu及中间层 Cu处于图 6中的 F 点，中间层中的 Mn处于 G 点，都呈固态粉末状。在一定压力的作用下，中间层 Mn与母材 Cu及中间层 Cu接触，Cu和 Mn之间就发生相互扩散，互扩散达到 $C_{\alpha s}$或 $C_{\gamma s}$时，接触界面处发生溶解现象。随着浓度的变化，CuMn液相量不断增加。当溶质原子浓度到达 $C_{\alpha L}$或 $C_{\gamma L}$时，扩散形成的合金全部熔化成液相。当中间层完全溶解时，阶段 I结束。该阶段结束的主要标志是不断出现液相，固 液边界一直在扩大，溶解过程主要受 Mn扩散率控制。

(2)液相均匀化阶段:当中间层 Cu、Mn完全溶解后,液相中 Mn浓度约为中间层百分比浓度 C_L。随着保温时间的延长,由于存在着从中间层液相到固 液边界的 Mn的正浓度梯度,液相中 Mn原子不断地向固 液边界扩散,促使母材 Cu的不断溶解。液相中 Mn原子平均浓度含量不断降低,Cu原子平均浓度不断提高,当液相浓度达到 $C_{\alpha L}$时,液相层达到了最大宽度,阶段 II结束。该阶段的主要标志是过渡液相层达到最大宽度,主要特征是母材不断溶解,液相层不断扩大,扩散完全受溶质原子在液相中的扩散率控制。

(3)等温凝固阶段:继续保温,由于液相和固相之间还存在 Mn的正浓度梯度,液相中的 Mn原子继续向固 液边界扩散,然后向母材扩散,当液相中的 Mn原子浓度小于 $C_{\alpha L}$时,该部分液相开始转化为固相,液 固界面向前推进,等温凝固形成 α相浓度 $C_{\alpha S}$,见图 6中 C点;液相中 Mn浓度仍保持在 B点处浓度 $C_{\alpha L}$,其数量逐渐减少,当液相中 Mn浓度达到图 6中 C点时,液相完全消失,等温凝固结束。该过程结束的主要标志是液相完全消失,主要特征是液 固界面不断地向前推进,母材 Cu一侧不断地出现固相,扩散主要受溶质原子在固相中扩散率主导,需要较长的时间。

(4)接头均匀阶段:等温凝固结束后,连接已经基本上完成,但是由于连接区域内 Mn原子的浓度还较高,对结构的完整性不利。因此,需继续保温,Mn原子进一步扩散,则开始均匀化过程,此时凝固部分 Cu、Mn的成分浓度从图 6中 C点向 D点转化,连接区域溶质趋于均匀。该过程需要更长时间,并且一般难以达到完全均匀化。

3 结 论

(1)采用两种不同的中间层即 67Cu-33Mn、67Cu-33Mn-5Ni(质量百分比)金属粉末,在连接温度为 890℃,保温时间为 480 min,压力 3 MPa工艺参数下,成功地实现了 W与 Cu合金的 TLP连接。结果表明,接头显微织致密且界面结合良好。

(2)Ni元素对接头的显微组织及界面结合起到了重要影响作用。一方面,Ni会提高 Cu元素向焊缝扩散的扩散率,使得 Cu、Mn扩散加快,加速等温凝固,增加接头均匀化时间,致使获得良好的接头;另一方面,Ni能溶解一定量的 W,形成 Ni(W)固溶体,提高了中 间层与母材 W界面的结合力。

(3)W与 Cu瞬时液相扩散连接的机理是,通过中间层 Cu-Mn形成液相,与母材 Cu实现 TLP扩散连接;与母材 W实现钎焊连接。

参考文献:

[1] 许增裕. 国际热核实验堆的建造与聚变堆材料研究[J]. 原子能科学技术, 2005, 39(增刊): 47-51.

[2] Merola M, Akiba M, Barabash V, *et al*. Overview on fabrication and joining of plasma facing and high heat flux materials for ITER [J]. Journal of Nuclear Materials, 2002, 307-311: 1524-1532.

[3] Saito S, Fukaya K, Ishiyama S, *et al*. Mechanical properties of HIP bonded W and Cu-alloys joint for plasma facing components [J]. Journal of Nuclear Materials, 2002, 307-311: 1542-1546.

[4] Smid I, Akiba M, Vieider G, *et al*. Development of tungsten armor and bonding to copper for plasma-interactive components [J]. Journal of Nuclear Materials, 1998, 258-263: 160-172.

[5] Davis J W, Slattery K T, Driemeyer D E, *et al*. Use of tungsten coating on ITER plasma facing components[J]. Journal of Nuclear Materials, 1996, 233-237: 604-608.

[6] Chapa J, Reimanis I. Modeling of thermal stresses in a graded Cu/W joint[J]. Journal of Nuclear Materials, 2002, 303: 131-136.

[7] Rigal E, Bucci P, Le Marois G. Fabrication of monoblock high heat flux components for ITER divertor upper vertical target using hot isostatic pressing diffusion welding[J]. Fusion Engineering and Design, 2002, 49-50: 317-322.

[8] 邹贵生, 赵文庆, 吴爱萍, 等. Ti和 Ti/Ni/Ti连接钨与铜及其合金的界面结合机制与接头强度[J]. 航空材料学报, 2004, 24(3): 36-42.

[9] Barabash V, Akiba M, Cardella A, *et al*. Armor and heat sink materials joining technologies development for ITER plasma facing components[J]. Journal of Nuclear Materials, 2000, 283-287: 1248-1252.

[10] 邹贵生, 吴爱萍, 高守传, 等. Ag_2Cu_2Ti活性钎料真空钎焊钨、石墨与铜的研究[J]. 新技术新工艺·材料与表面处理, 2002, (6): 40-42.

[11] 长崎 诚三, 平林 真. 二元合金状态图集[M]. 北京: 冶金工业出版社. 2004.

[12] Batra I S, Kale G B, Saha T K, *et al*. Diffusion bonding of Cu-CrZr alloy to stainless steel and tungsten using nickel as an interlayer[J]. Materials Science & Engineering A, 2004, 369: 119-123.

作者简介:沈以赴,男,1964年 12月生,工学博士,副教授。研究方向为异种材料连接技术、纳米材料烧结及激光快速成型,发表论文 40余篇。

Email: yifushen@nuaa.edu.cn

Abstract: According to the brazing techniques of large scale generators and high power transformers, a 20 kHz/40 kW superaudio frequency inverted welding power supply was dasigned. It used PSM (Pulse Symmetrical Modulated) power control inverter. The serial-resonant full bridge inverter executes both power converting and power adjusting. The main switches of the inverter are controlled according to the PSM and the inverter always works at resonant with the same pace of the load and work in shutting off at ZCS and ZVS while switching on and off. The inverter is with unity power factor and raises efficiency.

Key words: Welding; Inverter; ZCS; Exceed Audio Frequency Induction; Generator; Transformer

Mechanical properties and microstructure of TIG+MIG welded joint of T91 steel CHANG Tie-jun[1], GONG Zheng-chun[2], LI Zi-feng[1], WANG Chang-bai[1] (1. School of Mechanical and Electric Engineering, Harbin Engineering University, Harbin 150001, China; 2. Harbin Boiler Company Ltd., Harbin 150046, China). p59-61, 88

Abstract: The mechanical properties, creep strength and high temperature ageing of TIG+MIG welded joint of T91 steel were tested. Microstructure and fracture morphology of the joint was analyzed. The creep strength of 625 ℃ for 17 958 h is 70 MPa, which can deduce that the sustained strength after 10^5 h is 46.5 MPa and the FATT is -13 ℃. It is proved that the properties of TIG+MIG welding joint at high temperature is determined by the change of microstructure. Furthermore, $M_{23}C_6$ plays an important role.

Key words: T91 steel; FATT; microstructure; sustained strength

Investigation for SnAgCu/Cu and SnAgCu/Au/Ni/Cu surface mounted soldered joints stored at high temperature XUE Song-bai[1], WANG Xu-yan[1], YU Sheng-lin[2] (1. College of Materials Science & Technology, Nanjing University of Aeronautics & Astronautics, Nanjing 210016, China; 2. The 14th Research Institute, China Electronics Technology Group Corporation, Nanjing 210013, China). p62-64

Abstract: Shear strength and fracture photograms of SnAgCu/Cu and SnAgCu/Au/Ni/Cu surface mounted soldered joints stored at high temperature were investigated. Results indicate that the shear strength of SnAgCu/Cu and SnAgCu/Au/Ni/Cu soldered joints decrease with high temperature storage time increasing, and the shear strength of SnAgCu/Cu soldered joint is larger than that of SnAgCu/Au/Ni/Cu soldered joint. Analysis for fracture photograms of SnAgCu/Cu and SnAgCu/Au/Ni/Cu soldered joints indicates that most of the fractures of SnAgCu/Cu and SnAgCu/Au/Ni/Cu soldered joints occurred in the metallic layer of surface mounted components' ends and minority fractures occurred in the solder/pad interface or in the solder.

Key words: shear strength; Sn-Ag-Cu solder; soldered joint; storage at high temperature

Simulation of the temperature field and flow field in full penetration laser welding DU Han-bin[1], HU Lun-jf[2], WANG Dong-cuan[1], SUN Cheng-zhi[1] (1. Automotive Engineering Academy of Shanghai Automotive Industry Co. (Group), Shanghai 200437, China; 2. School of Materials Sci. & Eng., Huazhong University of Science and Technology, Wuhan 430074, China). p65-68, 100

Abstract: A three dimensional mathematical model for the temperature field and flow field in full penetration laser welding of titanium alloy was presented. In this model, the heat source comprises a plane heat source on the top surface and a cylindrical heat source along the z direction, which takes into account the plasma effect and the keyhole absorption. The mushy region is introduced to provide a simple method to dispose of the pressure and velocity boundary conditions. Calculated results from the models are found to agree with the experimental results for the geometry profile of weld. The metal flow is the main cause for forming the typical "hourglass" cross section profile.

Key words: laser welding; temperature field; flow field; mathematical simulation

Influence of cerium on microstructure of Sn-Ag-Cu lead-free solder CHEN Yan[1], XUE Song-bai[2], LV Xiao-chun[1], LIAO Yong-ping[1] (1. Harbin Welding Institute, Harbin 150080, China; 2. Nanjing University of Aeronautics and Astronautics, Nanjing 210016, China). p69-72

Abstract: The microstructures of Sn-3.8Ag-0.7Cu lead-free solder with different contents of cerium were studied. The studied results showed that the microstructures can be refined and the intermetallic compounds can be suppressed because of addition of small amounts of cerium into the lead-free solder. When cerium is 0.03wt%, the microstructure of the solder is fine and distributed uniformly, and which possess the best mechanical properties of soldered joints and better wettability. When cerium is over 0.03wt%, the black cerium-rich phase appears and increases with the content of cerium. The microstructure analyses and theoretical calculation indicated that the black cerium-rich phase is a compound of Sn and Ce.

Key words: cerium; lead-free solder; microstructure

Tansient liquid phase bonding tungsten to copper alloy SHEN Yi-fu[1], LIU Shi-fu[1], LI Jun-wei[2], XU Jie[1] (1. College of Materials Science and Technology, Nanjing University of Aeronautics and Astronautics, Jiangsu Nanjing 210016, China; 2. XiaMen Honglu Corporation, Fujian Xiamen 361021, China). p73-76

Abstract Transient liquid phase bonding of Tungsten (W) to copper (Cu) alloy using 67Cu-33Mn or 67Cu-33Mn-5Ni (mass fraction) as the interlayer was studied. The microstructures and chemical composition across the bond interface were analyzed by using SEM and EDX. The microstructure of TLP joint using 67Cu-33Mn-5Ni as the interlayer was denser than that of the TLP joint using 67Cu-33Mn as the interlayer. The addition of Ni plays an important role in increasing diffusion rate, isothermally solidification rate and in Ni(W) solid solution formation. The bonding mechanism of W to Cu alloy is found to be a combination of TLP bonding and brazing. The TLP acts as a feasible bonding mechanism of the Cu-Mn interlayer and the Cu alloy, while the brazing mechanism prevails between the interlayer and the W.

Key words transient liquid phase bonding; brazing; microstructures; mechanism

Wavelet transform algorithm of seam image process with DSP

HUANG Jun-fen[1], JIANG Li-pei[1], ZOU Yong[1], YIN Shu-yan[2] (1. Optomechatronic Beijing Area Major Laboratory, Beijing Institute of Petrochemical Technology, Beijing 102617, China; 2. College of Material Science and Engineering, Beijing University of Technology, Beijing 100022, China). p77 - 80

Abstract The position of seam center was got with template match algorithm. First seam template was acquired through wavelet transform, then the template was shifted in subsequent seam image and correlation coefficients were calculated accordingly, the column corresponding to the max correlation coefficient was taken as seam center position of subsequent seam image. The seam image is processed with TDS642EVM since DSP has advantages in digital signal processing. Principle of 2-D wavelet transform algorithm was analyzed, then wavelet transform programs on DSP are developed. At last, example of processing pipeline seam image with TDS642EVM was given.

Key words seam image process; 2D wavelet transform; DSP

New heat source model for numerical simulation of electron beam welding

WANG Xi-chang, WU Bing, ZUO Cong-jia, LIU Fang-jun (Beijing Aeronautical Manufacturing Technology Research Institute, National Key Laboratory For High Density Beam Processing technology, Beijing 100024, China). p81 - 84

Abstract Rotary-Gauss body heat source model can show appropriately the character of electron beam deep penetration welding, but only smooth "parabola" shape weld can be obtained. It is improved to reflect general "wine cup" or "nail" shape weld, and also numerically simulated temperature field distributions during electron beam welding of plate by using ANSYS, and it was validated with weld profile and thermal cycle curves measured. The results of calculations is in a good agreement with the experiment.

Key words electron beam welding; heat source model; temperature field; weld profile; thermal cycle curves

Finite element analysis on reliability of soldered joint of J-lead

WU Yu-xiu, XUE Song-bai, HU Yong-Fang (College of Materials Science & Technology, Nanjing University of Aeronautics & Astronautics, Nanjing 210016, China). p85 - 88

Abstract Finite element method was used to simulate the soldered joint of J-lead of the SOJ (Small Outline J-lead Package). Results indicate that the distortion is obvious, the ceramic carrier with upwarp trend, the J-lead with forth extension trend, but the PCB with little distortion because of the rigidity displacement restrict. The strain of the J-lead soldered joint′s soldered heel is bigger than the soldered toe and the center place has the least strain. The stress of the J-lead soldered heel is bigger than the other place of the soldered joint and the stress distributes a wide area, where is the weakest place of the whole soldered joint, so it is easy to lose efficacy. The stress of the J-lead soldered toe is less than the soldered heel, and the stress distributing area is small. On the contrary, the J-lead soldered joint′s center place distributes a large area and the stress value is one order less than the stress value of soldered heel and soldered toe, so it is the safety place of the soldered joint. The calculated values are in agreement with the experimental results.

Key words SOJ; stress; soldered joint; finite element

Microstructure analyse of surface Ti-metallized graphite

LIU Shi-fu, SHEN Yi-fu, WANG Shao-gang (College of Materials Science and Technology, Nanjing University of Aeronautics and Astronautics, Nanjing 210016, China). p89 - 92

Abstract The microstructure of surface Ti-metallized graphite was analyzed by XRD, SEM and EDX. The results show that the surface Ti-metallized graphite consists of interior layer (graphite), transition layer (620μm), dense layer (40μm) and exterior layer (Ti). XRD and EDX results show titanium carbide phase in the dense layer. SEM analyses confirm that good bonding exist between the interfaces. The short micro-structural crack between titanium and dense layer was found due to the large difference in the coefficient of thermal expansion. The crack can be eliminated by furnace cooling instead of air cooling. It was not found between dense layer and transition layer because of titanium carbide deformed by the Ti-C reaction.

Key words graphite; titanium; metallization; microstructure

Establishment of fatigue Fractal damage evolution equation on TC11